Research Square

Preprints are preliminary reports that have not undergone peer review.
They should not be considered conclusive, used to inform clinical practice,
or referenced by the media as validated information.

A simple analytical solution for the evolution of the mean eccentricity vector in extremely low lunar orbits

Ana S. Rivero

asanchez8@us.es

Universidad de Sevilla

Giulio Baù

Universita degli Studi di Pisa https://orcid.org/0000-0002-9857-0866

Rafael Vazquez

Universidad de Sevilla

Research Article

Keywords: Lunar orbital dynamics, non-zonal harmonics, eccentricity vector

Posted Date: November 24th, 2026

DOI: https://doi.org/10.21203/rs.3.rs-11829832/v1

License: This work is licensed under a Creative Commons Attribution 4.0 International License.
Read Full License

Additional Declarations: The authors declare no competing interests.

A simple analytical solution for the evolution of the mean eccentricity vector in extremely low lunar orbits

Ana S. Rivero[1*], Giulio Baù[2] and Rafael Vazquez[1]

[1]Escuela Técnica Superior de Ingeniería, Universidad de Sevilla, Camino de los Descubrimientos s.n., Sevilla, 41092, Spain.
[2]Department of Mathematics, Università di Pisa, Largo Pontecorvo, 5, Pisa, 56127, Italy.

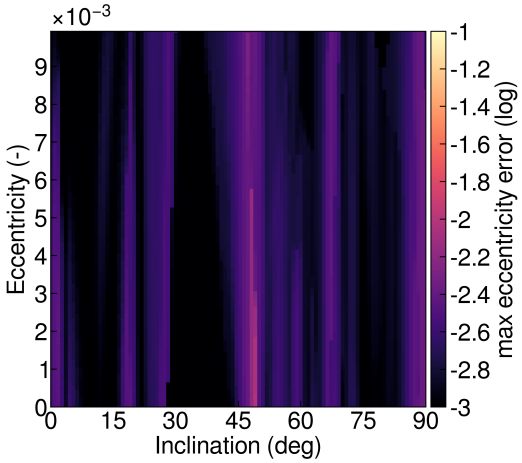
*Corresponding author(s). E-mail(s): asanchez8@us.es;
Contributing authors: giulio.bau@unipi.it; rvazquez1@us.es;

Abstract

Orbital dynamics in extremely Low Lunar Orbits (eLLOs), whose altitudes are typically lower than 50 km, is dominated by the Moon's gravity field, where the presence of "mascons" can cause instabilities of the motion and lead satellites to collide with the lunar surface. This work presents a compact analytical solution for the evolution of the mean eccentricity vector of near-circular eLLOs under the effect of zonal, sectorial and tesseral harmonics of the lunar gravity field. It represents an extension of the theories by G.E. Cook (1966) and R.A. Cook (1992), who considered only zonal harmonics. The analytical model is validated against numerical propagations of a broad set of initial conditions, showing that it reproduces the main long- and medium-period features of the mean eccentricity vector as long as the assumptions of the model remain satisfied. The results highlight the importance of odd-degree tesseral harmonics in shaping the eccentricity evolution and support the use of this model as a complementary tool for understanding and predicting the motion of near-circular eLLOs.

Keywords: Lunar orbital dynamics, non-zonal harmonics, eccentricity vector

Graphical Abstract



1 Introduction

Extremely Low Lunar Orbits (eLLOs), typically at altitudes below 50 km, are of particular interest for applications requiring close proximity to the lunar surface, such as high-resolution imaging and geophysical observations [1]. The dominant perturbation affecting these orbits is the Moon's nonspherical gravity field. Its complex internal structure and surface topography produce substantial departures from spherical symmetry, including pronounced longitudinal variations, so accurate orbit prediction requires a sufficiently detailed spherical-harmonic representation. An early contribution was made by Konopliv et al. [2], who developed a lunar gravity model through degree and order 60 and investigated its implications for predicted orbital behavior. Truncations at degree and order 50 have subsequently been used in low-lunar-orbit studies [3–5], although the required truncation depends on the orbit and the accuracy sought. Third-body perturbations from the Earth and the Sun are generally secondary to lunar nonspherical gravity in the extremely low-altitude regime considered here [1].

Non-zonal (i.e., sectorial and tesseral) harmonics can significantly affect the eccentricity of eLLOs and therefore their risk of impact with the lunar surface. Previous studies have examined individual harmonic contributions to near-circular mapping orbits and the selection of favorable orbital configurations [4, 6–8]. Within a simplified lunar gravity model, Meyer et al. [7] identified substantial medium-period eccentricity variations associated with C_{31}, superimposed on the long-period effects of odd zonal harmonics such as J_3 and J_5. Ramanan and Adimurthy [4] identified C_{70}, C_{90}, and C_{91} as important contributors to perilune evolution in the cases they studied, and emphasized the need to include non-zonal terms in orbit-lifetime and maintenance analyses.

Folta and Quinn [9] combined an analytical formulation with numerical simulations to investigate lunar frozen orbits under lunar gravity and third-body perturbations, emphasizing the restrictions imposed by lunar mascons and the Earth–Moon geometry. Russell and Lara [10] subsequently computed long-lifetime repeat ground-track orbits

using a high-degree and high-order lunar gravity field combined with the Earth–Moon restricted three-body model. These studies illustrate why the design of low lunar orbits must account for the longitudinal structure of the lunar gravity field as well as its zonal component.

A particularly useful manifestation of non-zonal perturbations is the approximately repeatable monthly pattern traced by the eccentricity vector of near-circular low lunar orbits. This feature, known as the "translation theorem", was described by Beckman and Lamb [11] during the planning of stationkeeping operations for the Lunar Reconnaissance Orbiter. For fixed semi-major axis, inclination, and initial nodal longitude relative to the Moon, changing the initial eccentricity vector approximately translates this pattern without altering its shape. Yarndley et al. [1] provided an analytical explanation of this behavior, identifying the dominant role of a subset of odd-degree sectorial and tesseral harmonics.

The orbital elements are the parameters describing the size, shape and orientation of the orbit and the position of the satellite along it. Their variations are classified by time scale: short-period variations occur within about one orbital revolution, long-period variations evolve over many orbital revolutions, and secular variations are non-periodic drifts that accumulate over time. The monthly modulations described above are medium-period variations, intermediate between the short- and long-period ones and the main focus of this work. In particular, the rotation-related contributions associated with harmonics of order m, commonly referred to as m-monthly terms, have characteristic periods of approximately $T_{\leftmoon}/m$, with corrections due to nodal precession, where $T_{\leftmoon} = 27.321661$ days is the lunar sidereal month [1]. Unlike the short-period terms, these contributions survive averaging over the satellite's mean anomaly and can produce substantial eccentricity variations relevant to orbit maintenance and impact avoidance [4, 11].

Several analytical and semi-analytical models have been developed to describe lunar satellite motion. Their formulations differ in the perturbations retained and in the averaging and solution procedures adopted. Without attempting an exhaustive review, we highlight some representative contributions. The analytical theory developed by Knežević and Milani [12, 13] describes low-altitude, nearly polar lunar orbits using a spherical-harmonic representation of the lunar gravity field. The implementation encounters practical limitations for degrees above approximately 40. In their theory, the long-period part of the averaged disturbing function contains only the zonal harmonics; truncated at second order in the eccentricity, it yields linear differential equations with constant coefficients for the components of the eccentricity vector, an approximation that the authors note is consistent only for nearly polar orbits. The medium-period effects of the non-zonal harmonics, with periods shorter than one lunar month, are removed through a canonical transformation between mean and osculating elements. In contrast, the formulation proposed here is not restricted to nearly polar orbits, and it retains the medium-period forcing of the odd-degree non-zonal harmonics in the mean-element equations, which are solved in closed form together with the zonal long-period dynamics. Lara et al. [14] developed an analytical averaging theory incorporating a 50-degree zonal gravity model and third-body effects for

low-altitude polar orbits. Mastroianni et al. [15] implemented a fully analytical propagator including twelve dominant lunar gravity harmonics together with the Earth's quadrupole tidal perturbation, applicable over an altitude range of approximately 300–3000 km. Mahajan [16] developed a formulation accommodating spherical harmonics of arbitrary degree and order, including second-order secular and long-period contributions arising from their mutual coupling, together with first-order secular effects of third-body perturbations.

Among semi-analytical approaches, De Saedeleer [17] derived a Hamiltonian averaging theory that removes only the short-period terms and accounts for lunar rotation, the J_2 and C_{22} harmonics, and the Earth's perturbations. San-Juan et al. [18] obtained a closed-form semi-analytical theory for LLOs considering a 50×50 lunar gravity field together with the Earth's attraction. Efthymiopoulos et al. [19] developed SELENA, a semi-analytical propagator using a 10×10 lunar gravity model along with additional perturbations. Using a related closed-form secular model, Legnaro and Efthymiopoulos [20] investigated eccentricity growth and orbital lifetimes, primarily at higher altitudes, and emphasized the difficulty of constructing an accurate averaged description below approximately 100 km, where many higher-degree harmonics contribute. More recently, Lara [21] showed, using a 3×3 gravity model, that coupling between non-zonal harmonics can modify the averaged dynamics even for nonresonant lunar orbits.

Incorporating a 50×50 gravity model into perturbation-based theories can entail substantial algebraic complexity, particularly when constructing the transformations needed to recover short- and medium-period effects. Simpler analytical solutions that approximate the eccentricity-vector evolution are therefore of interest. G.E. Cook [22] considered the effects of the dominant terrestrial zonal harmonic J_2 and odd zonal harmonics on the eccentricity vector of near-circular satellites. The Lagrange equations for the non-singular projections

$$\xi = e\cos\omega, \qquad \eta = e\sin\omega, \tag{1}$$

where e is the eccentricity and ω the argument of perilune, were reduced to a linear system with constant coefficients and solved explicitly. A solution $(\xi(t), \eta(t))$ describes a circle at a constant angular frequency about an equilibrium whose position is determined by the forcing due to odd zonal harmonics. The argument of pericenter can either circulate or librate, depending on whether the origin lies inside or outside the circle, respectively. R.A. Cook [23] extended this formulation to include all even and odd zonal harmonics while retaining a linear system with constant coefficients. The resulting motion can be either oscillatory or hyperbolic; in the oscillatory case, the eccentricity vector traces an ellipse periodically. Deleflie et al. [24] combined the long-period solution of Cook [23][1] with first-order periodic corrections for a gravity field of arbitrary degree and order. Their formulation was demonstrated for Earth satellites using a 10×10 gravity field. Its accuracy for eLLOs requires assessment because non-zonal contributions can be comparable to the zonal effects.

[1] See also Deleflie et al. [25] for an independent derivation of the long-period solution.

In this work, we propose a simple formulation for the evolution of the *mean* (i.e., after removing short-period terms) eccentricity vector of near-circular eLLOs under a lunar gravity field truncated at arbitrary degree and order. We extend the formulations of G.E. Cook and R.A. Cook [22, 23] to include non-zonal harmonics. The resulting linear system has time-dependent coefficients. To obtain a compact closed-form approximation, we assume constant inclination and prescribed linear nodal precession, retain the zonal coupling coefficients and the explicit forcing due to odd-degree non-zonal harmonics, and neglect the even-degree non-zonal modulation of the homogeneous coefficients. The accuracy and limitations of these assumptions are assessed numerically. The proposed formulation is intended to complement existing analytical and semi-analytical propagators.

The article is organized as follows: Section 2 develops the disturbing function. Section 3 derives the equations governing the eccentricity-vector evolution. Section 4 presents the analytical solution, yielding closed-form expressions for its components. Section 5 assesses the model through numerical simulations and examines its applicability. Finally, Section 6 summarizes the findings and outlines directions for future research.

2 Development of the disturbing function

The disturbing function due to the nonspherical gravity field of the central body is expressed as a function of the classical orbit elements as [see 26]:

$$U = \frac{\mu}{a} \sum_{l=2}^{\infty} \left(\frac{R_{\leftmoon}}{a} \right)^{l} \sum_{m=0}^{l} \sum_{p=0}^{l} F_{lmp}(I) \sum_{q=-\infty}^{\infty} G_{lpq}(e) S_{lmpq}(\omega, M, \Omega, \theta), \tag{2}$$

where

$$S_{lmpq} = \begin{Bmatrix} C_{lm} \\ -S_{lm} \end{Bmatrix}_{l-m \text{ odd}}^{l-m \text{ even}} \cos \Psi_{lmpq} + \begin{Bmatrix} S_{lm} \\ C_{lm} \end{Bmatrix}_{l-m \text{ odd}}^{l-m \text{ even}} \sin \Psi_{lmpq}, \tag{3}$$

and the argument Ψ_{lmpq} is defined by the combination of angles

$$\Psi_{lmpq} = (l - 2p)\,\omega + (l - 2p + q)\,M + m\,(\Omega - \theta)\,. \tag{4}$$

In (2), $\mu = GM_{\leftmoon}$ with G the gravitational constant and $M_{\leftmoon}$ the mass of the Moon, $R_{\leftmoon}$ is the mean radius of the Moon, $(a, e, I, \omega, \Omega, M)$ are the classical orbital elements: semi-major axis, eccentricity, inclination, argument of pericenter, longitude of the ascending node and mean anomaly, respectively. Moreover, θ represents the sidereal rotation angle of the Moon. The terms C_{lm} and S_{lm} are the dimensionless spherical-harmonic coefficients characterizing the mass distribution of the Moon. The expression for S_{lmpq} uses a standard case-wise notation where the harmonic coefficients preceding the cosine and sine terms are selected based on whether $l - m$ is even or odd, as indicated by the conditions next to the curly braces.

The functions F_{lmp} and G_{lpq} are the inclination and eccentricity functions [see 26, 27]. The inclination function can be written as

$$\begin{aligned} F_{lmp}(I) = & \sum_{t=0}^{\min\{p,k\}} \frac{(2l-2t)!}{2^{2l-2t}\, t!\, (l-t)!\, (l-m-2t)!} \sin^{l-m-2t} I \\ & \times \sum_{s=0}^{m} \binom{m}{s} \cos^{s} I \sum_{c=c_0}^{c_1} \binom{l-m-2t+s}{c} \binom{m-s}{p-t-c} (-1)^{c-k}, \end{aligned} \tag{5}$$

where[2]

$$k = \left\lfloor \frac{l-m}{2} \right\rfloor$$

and

$$\begin{aligned} c_0 &= \max\{0,\ p-t-m+s\}, \\ c_1 &= \min\{l-m-2t+s,\ p-t\}. \end{aligned}$$

The eccentricity functions are related to Hansen coefficients [see 28, §95] by

$$G_{lpq}(e) = X_{(l-2p+q)}^{-(l+1),(l-2p)}(e). \tag{6}$$

The explicit expressions of the inclination and eccentricity functions, $F_{lmp}(I)$ and $G_{lpq}(e)$, are tabulated for example in Kaula [26] and Cayley [29].

Since only the medium- and long-period terms are considered here, the terms in Eq. (2) that depend on the mean anomaly, M, are eliminated. Therefore, the following condition must be satisfied:

$$l - 2p + q = 0. \tag{7}$$

After this elimination, we switch from *osculating* to *mean* orbital elements. From Eq. (6) and condition (7) Hansen coefficients are computed by the relation [see 30, Eq. 26]

$$\begin{aligned} X_0^{-(l+1),(l-2p)} = & \left(1+\beta^2\right)^l \left(1-\beta^2\right)^{1-2l} (-\beta)^{l-2p} \binom{-2p}{l-2p} \\ & \times F\left(1-2p, 1-l; l-2p+1; \beta^2\right), \end{aligned}$$

where F is the hypergeometric function and

$$\beta = \frac{e}{1+\left(1-e^2\right)^{1/2}}.$$

Note that, if $e \neq 0$, the eccentricity function vanishes for $p = 0, l$. Moreover, as the eccentricity function G_{lpq} is of the order of $O(e^{|q|})$, only terms in the summation over q corresponding to

$$|q| \leq 2 \tag{8}$$

[2] The symbol $\lfloor x \rfloor$ denotes the greatest integer less than or equal to x.

are retained in the present first-order analytical theory.

3 Equations of motion

Let us denote by $\overline{U}_{(2)}$ the averaged disturbing function with the further restrictions $l \leq l_{\max}$, $|q| \leq 2$. For convenience, the mean orbital elements are denoted with the same symbols as the osculating ones. Since $\overline{U}_{(2)}$ is independent of the mean anomaly, the mean semi-major axis is constant. Moreover, we have

$$\begin{aligned}
\dot{e} &= -\frac{\sqrt{1-e^2}}{\alpha e}\frac{\partial \overline{U}_{(2)}}{\partial \omega}, \\
\dot{\omega} &= \frac{\sqrt{1-e^2}}{\alpha e}\frac{\partial \overline{U}_{(2)}}{\partial e} - \frac{\cot I}{\alpha\sqrt{1-e^2}}\frac{\partial \overline{U}_{(2)}}{\partial I}, \\
\dot{I} &= -\frac{1}{\alpha\sqrt{1-e^2}\sin I}\frac{\partial \overline{U}_{(2)}}{\partial \Omega} + \frac{\cot I}{\alpha\sqrt{1-e^2}}\frac{\partial \overline{U}_{(2)}}{\partial \omega}, \\
\dot{\Omega} &= \frac{1}{\alpha\sqrt{1-e^2}\sin I}\frac{\partial \overline{U}_{(2)}}{\partial I},
\end{aligned} \tag{9}$$

with $\alpha = \sqrt{\mu a}$. This paper addresses the medium- and long-period effects on the evolution of e and ω due to all spherical harmonics up to an arbitrary order and degree $l_{\max}$. Two relevant assumptions are made to model the behavior of the other two variables Ω and I. First, we assume that the inclination remains always equal to its mean value computed at the initial epoch of the propagation time-window. Section 5 will show the impact of this simplification of our model on its accuracy. Then, since within the first-order averaged theory developed here, odd zonal and non-zonal harmonics generically introduce small oscillatory corrections to the motion of Ω, we assume that this angle evolves linearly in time with a constant secular frequency driven by all even zonal harmonics in the range $0 \leq l \leq l_{\max}$:

$$h_{\text{sec}} = \frac{n}{\sin I\sqrt{1-e^2}} \sum_{s=1}^{\lfloor l_{\max}/2 \rfloor} \left(\frac{R_{\leftmoon}}{a}\right)^{2s} F'_{2s,0,s}(I)\, G_{2s,s,0}(e)\, C_{2s,0}, \tag{10}$$

where $n = \sqrt{\mu/a^3}$ is the satellite's mean motion, and $'$ denotes the derivative with respect to I. Note that in Eq. (10) the eccentricity takes its mean value at the initial epoch.

Consequently, the analysis focuses on the two equations that govern the evolution of the mean eccentricity vector on the orbital plane: $\dot{e}$ and $\dot{\omega}$. It is well-known that the singularity $e = 0$ can be removed from these equations by introducing the projections ξ and η defined in Eq. (1), whose time derivatives take the form

$$\dot{\xi} = \frac{1}{\alpha}\left[-\frac{\sqrt{1-e^2}}{e}\frac{\partial \overline{U}_{(2)}}{\partial \omega}\cos\omega - \left(\sqrt{1-e^2}\frac{\partial \overline{U}_{(2)}}{\partial e} - \frac{e}{\sqrt{1-e^2}}\cot I\frac{\partial \overline{U}_{(2)}}{\partial I}\right)\sin\omega\right],$$

$$\dot{\eta} = \frac{1}{\alpha}\left[-\frac{\sqrt{1-e^2}}{e}\frac{\partial \overline{U}_{(2)}}{\partial \omega}\sin\omega + \left(\sqrt{1-e^2}\frac{\partial \overline{U}_{(2)}}{\partial e} - \frac{e}{\sqrt{1-e^2}}\cot I \frac{\partial \overline{U}_{(2)}}{\partial I}\right)\cos\omega\right].$$

3.1 Contributions of the even-degree harmonics

This section details the contribution of even-degree harmonics: the degree l is restricted to even values, and since all orders up to $l_{\max}$ are considered, $0 \leq m \leq l$. In light of conditions (7), (8), we have

$$\begin{aligned} q &\in E = \{-2, 0, 2\}, \\ p &= \frac{l+q}{2}. \end{aligned}$$

The generic term of degree l, with l even, and order m of $\overline{U}_{(2)}$ is expressed as

$$\overline{U}_{(2)lm} = \frac{\mu}{a}\left(\frac{R_{\mathbb{Q}}}{a}\right)^l \sum_{q\in E} F_{lm\frac{l+q}{2}}(I) G_{l\frac{l+q}{2}q}(e) S_{lm\frac{l+q}{2}q}(\omega, \Omega, \theta),$$

where from Eqs. (3), (4),

$$S_{lm\frac{l+q}{2}q} = \begin{Bmatrix} C_{lm} \\ -S_{lm} \end{Bmatrix}_{l-m \text{ odd}}^{l-m \text{ even}} \cos\phi_{qm} + \begin{Bmatrix} S_{lm} \\ C_{lm} \end{Bmatrix}_{l-m \text{ odd}}^{l-m \text{ even}} \sin\phi_{qm} \tag{11}$$

and

$$\phi_{qm} := \Psi_{lm\frac{l+q}{2}q} = q\omega + m\left(\Omega - \theta\right).$$

Therefore, the eccentricity functions appearing in $\overline{U}_{(2)}$ are

$$\begin{aligned} G_{l\frac{l-2}{2}-2}(e) = X_0^{-(l+1),2}(e) &= \frac{(l-1)(l-2)}{8}e^2, \\ G_{l\frac{l}{2}0}(e) = X_0^{-(l+1),0}(e) &= 1 + \frac{l(l+1)}{4}e^2, \\ G_{l\frac{l+2}{2}2}(e) = X_0^{-(l+1),-2}(e) &= \frac{(l-1)(l-2)}{8}e^2 \end{aligned}$$

and their derivatives read

$$\begin{aligned} G'_{l\frac{l-2}{2}-2}(e) = G'_{l\frac{l+2}{2}2}(e) &= \frac{(l-1)(l-2)}{4}e, \\ G'_{l\frac{l}{2}0}(e) &= \frac{l(l+1)}{2}e, \end{aligned}$$

The contributions to $\dot{\xi}$ and $\dot{\eta}$ of the spherical harmonic of even degree l and order m are given by

$$\dot{\xi}_{lm} = n\left(\frac{R_{\leftmoon}}{a}\right)^l \left[-M^-_{lm,2}(I)\tilde{\mathcal{S}}_{lm}(\Omega,\theta)\xi + \big(M^+_{lm,2}(I) + N_{lm}(I)\big)\mathcal{S}_{lm}(\Omega,\theta)\eta\right], \tag{12}$$

$$\dot{\eta}_{lm} = n\left(\frac{R_{\leftmoon}}{a}\right)^l \left[M^-_{lm,2}(I)\tilde{\mathcal{S}}_{lm}(\Omega,\theta)\eta + \big(M^+_{lm,2}(I) - N_{lm}(I)\big)\mathcal{S}_{lm}(\Omega,\theta)\xi\right], \tag{13}$$

where we introduced the notation

$$M^\pm_{lm,2}(I) = \frac{(l-1)(l-2)}{4} f^\pm_{lm,2}(I),$$
$$f^\pm_{lm,2}(I) = F_{lm\,\frac{l-2}{2}}(I) \pm F_{lm\,\frac{l+2}{2}}(I),$$

$$N_{lm}(I) = F'_{lm\,\frac{l}{2}}(I)\cot I - \frac{l(l+1)}{2} F_{lm\,\frac{l}{2}}(I),$$

and

$$\mathcal{S}_{lm}(\Omega,\theta) = \begin{pmatrix} C_{lm} \\ -S_{lm} \end{pmatrix}^{m\text{ even}}_{m\text{ odd}} \cos\left(m(\Omega-\theta)\right) + \begin{pmatrix} S_{lm} \\ C_{lm} \end{pmatrix}^{m\text{ even}}_{m\text{ odd}} \sin\left(m(\Omega-\theta)\right),$$

$$\tilde{\mathcal{S}}_{lm}(\Omega,\theta) = \begin{pmatrix} S_{lm} \\ C_{lm} \end{pmatrix}^{m\text{ even}}_{m\text{ odd}} \cos\left(m(\Omega-\theta)\right) + \begin{pmatrix} -C_{lm} \\ S_{lm} \end{pmatrix}^{m\text{ even}}_{m\text{ odd}} \sin\left(m(\Omega-\theta)\right).$$

The combinations $f^\pm_{lm,2}$ are introduced to express the paired contributions with indices $p = (l-2)/2$ and $p = (l+2)/2$ in a compact form.

Remark 1 For even $l \geq 2$ and $0 \leq m \leq l$, $f^\pm_{lm,2}$ admit an equivalent representation in terms of derivatives of Legendre polynomials. The following identities are derived from the general inclination function formula of Gooding and Wagner [31, Eq. (4)], after conversion to Kaula's sign convention as discussed in their Sect. 3. Let

$$C_I = \cos I, \qquad S_I = \sin I, \qquad R_{lm}(x) = \frac{d^m P_l(x)}{dx^m}, \tag{14}$$

where P_l is the Legendre polynomial of degree l, and define

$$A_{lm} = \frac{2(-1)^{\lfloor m/2 \rfloor} P_l(0)}{(l-1)(l+2)}.$$

For $2 \leq m \leq l$, we obtain

$$f^+_{lm,2} = A_{lm} S_I^{m-2}\left[2C_I S_I^2 R'_{lm} + \Big(2m(m-1) - \big(l(l+1) - 2m\big)S_I^2\Big) R_{lm}\right],$$
$$f^-_{lm,2} = 2mA_{lm} S_I^{m-2}\left[(m-1)C_I R_{lm} - S_I^2 R'_{lm}\right],$$

where primes denote differentiation with respect to x and $x = C_I$. The remaining cases reduce to

$$f^+_{l0,2} = A_{l0} S_I^2 P''_l, \qquad\qquad f^-_{l0,2} = 0,$$

$$f^{+}_{l1,2} = A_{l1} S_I \left[2C_I P_l'' - \big(l(l+1) - 2\big) P_l'\right], \qquad f^{-}_{l1,2} = -2A_{l1} S_I P_l''.$$

These identities provide a compact alternative to the general inclination function formulas when only these paired contributions are required. Moreover, the representation involves only polynomials and remains regular at the equatorial inclinations $I = 0, \pi$.

Remark 2 Eqs. (12) and (13) contain products involving $\cot I$, which is singular at $I = 0, \pi$. The regularity of these products must therefore be examined explicitly. For even $l \geq 2$, the apparent singularity of $F'_{lm,\frac{l}{2}}(I)\cot I$ is removable for $m = 0$ and $m \geq 2$, whereas the isolated product diverges for $m = 1$.

Setting $m = 0$ and $p = l/2$ in Eq. (5), the sum over s reduces to the single term $s = 0$. Moreover, the binomial coefficient $\binom{m-s}{p-t-c} = \binom{0}{p-t-c}$ vanishes unless $c = p - t = l/2 - t$. Hence,

$$F_{l0\frac{l}{2}}(I) = \sum_{t=0}^{l/2} (-1)^t \frac{(2l-2t)!}{t!(l-t)!2^{2l-2t}(l-2t)!} \binom{l-2t}{l/2-t} \sin^{l-2t} I.$$

Since l is even, every exponent $l - 2t$ is even. Thus, $F_{l0\frac{l}{2}}(I)$ is a polynomial in $\sin^2 I$. Differentiating gives

$$F'_{l0\frac{l}{2}}(I) = \sin I \cos I \sum_{t=0}^{l/2-1} (-1)^t \frac{(2l-2t)!(l-2t)}{t!(l-t)!2^{2l-2t}(l-2t)!} \binom{l-2t}{l/2-t} \sin^{l-2t-2} I.$$

Consequently, the factor $\sin I$ cancels with the denominator in $\cot I$, yielding

$$\cot I\, F'_{l0\frac{l}{2}}(I) = \cos^2 I \sum_{t=0}^{l/2-1} (-1)^t \frac{(2l-2t)!(l-2t)}{t!(l-t)!2^{2l-2t}(l-2t)!} \binom{l-2t}{l/2-t} \sin^{l-2t-2} I.$$

The right-hand side is regular throughout $[0, \pi]$. Evaluating this expression avoids computing the vanishing derivative and the singular cotangent separately.

The cancellation is not restricted to zonal harmonics. For even l, specializing Eq. (4) in Gooding and Wagner [31] to $p = l/2$ and collecting the half-angle factors yields

$$F_{lm\frac{l}{2}}(I) = (\sin I)^m Q_{lm}(\cos I),$$

where

$$Q_{lm}(x) = (-1)^{\lfloor m/2 \rfloor} P_l(0) \frac{d^m P_l(x)}{dx^m}$$

is a polynomial. For $m \geq 1$, differentiation gives

$$F'_{lm\frac{l}{2}}(I)\cot I = (\sin I)^{m-2}\Big[m\cos^2 I\, Q_{lm}(\cos I) - \sin^2 I \cos I\, Q'_{lm}(\cos I)\Big],$$

where the prime on Q_{lm} denotes differentiation with respect to its argument. For $m \geq 2$, this expression contains only nonnegative powers of $\sin I$ and is therefore regular at $I = 0, \pi$.

However, for $m = 1$,

$$F_{l1\frac{l}{2}}(I) = a_l I + O(I^3), \qquad a_l = \frac{l(l+1)}{2} P_l(0) \neq 0, \tag{15}$$

so that

$$\cot I\, F'_{l1\frac{l}{2}}(I) = \frac{a_l}{I} + O(I), \qquad I \to 0^+, \tag{16}$$

$$\cot I\, F'_{l1,\frac{l}{2}}(I) = -\frac{a_l}{\pi - I} + O(\pi - I), \qquad I \to \pi^-. \tag{17}$$

Thus, $m = 1$ is the only order for which we have a singularity.

Since $\cot I$ appears in the equation for $\dot{\omega}$, the singularity reflects the indeterminacy of the ascending node and the argument of pericenter for equatorial orbits. It is therefore a coordinate singularity, rather than a singularity of the gravitational potential.

3.2 Contributions of the odd-degree harmonics

This section details the contribution of odd-degree harmonics: the degree l is restricted to odd values and $0 \leq m \leq l$. In light of conditions (7), (8), we have

$$q \in O = \{-1, 1\},$$
$$p = \frac{l+q}{2}.$$

The generic term of degree l, with l odd, and order m of $\overline{U}_{(2)}$ is expressed as

$$\overline{U}_{(2)lm} = \frac{\mu}{a}\left(\frac{R_{\leftmoon}}{a}\right)^l \sum_{q\in O} F_{lm\frac{l+q}{2}}(I) G_{l\frac{l+q}{2}q}(e) S_{lm\frac{l+q}{2}q}(\omega, \Omega, \theta),$$

where $S_{lm\frac{l+q}{2}q}$ takes the expression in (11). The eccentricity functions of interest, are given by

$$G_{l\frac{l-1}{2}-1}(e) = X_0^{-(l+1),1}(e) = \frac{l-1}{2}e,$$
$$G_{l\frac{l-1}{2}1}(e) = X_0^{-(l+1),-1}(e) = \frac{l-1}{2}e$$

and their derivatives are

$$G'_{l\frac{l-1}{2}-1}(e) = G'_{l\frac{l-1}{2}-1}(e) = \frac{l-1}{2}.$$

The spherical harmonic of odd degree l and order m contributes to $\dot{\xi}$ and $\dot{\eta}$ as follows:

$$\dot{\xi}_{lm} = -n\left(\frac{R_{\leftmoon}}{a}\right)^l M^-_{lm,1}(I)\mathcal{S}^*_{lm}(\Omega, \theta), \tag{18}$$
$$\dot{\eta}_{lm} = n\left(\frac{R_{\leftmoon}}{a}\right)^l M^+_{lm,1}(I)\tilde{\mathcal{S}}^*_{lm}(\Omega, \theta), \tag{19}$$

where

$$\mathcal{S}^*_{lm}(\Omega, \theta) = \begin{pmatrix} C_{lm} \\ S_{lm} \end{pmatrix}^{m \text{ even}}_{m \text{ odd}} \cos\left(m(\Omega - \theta)\right) + \begin{pmatrix} S_{lm} \\ -C_{lm} \end{pmatrix}^{m \text{ even}}_{m \text{ odd}} \sin\left(m(\Omega - \theta)\right),$$

$$\tilde{\mathcal{S}}^*_{lm}(\Omega, \theta) = \begin{pmatrix} -S_{lm} \\ C_{lm} \end{pmatrix}^{m \text{ even}}_{m \text{ odd}} \cos\left(m(\Omega - \theta)\right) + \begin{pmatrix} C_{lm} \\ S_{lm} \end{pmatrix}^{m \text{ even}}_{m \text{ odd}} \sin\left(m(\Omega - \theta)\right)$$

and

$$M^\pm_{lm,1}(I) = \frac{(l-1)}{2} f^\pm_{lm,1}(I),$$

$$f^{\pm}_{lm,1}(I) = F_{lm\,\frac{l-1}{2}}(I) \pm F_{lm\,\frac{l+1}{2}}(I).$$

For odd l, the combinations $f^{\pm}_{lm,1}$ group the inclination functions with indices $p = (l-1)/2$ and $p = (l+1)/2$. Their sum and difference allow the paired contributions to the equations of motion to be expressed in a compact form.

Remark 3 The combinations $f^{\pm}_{lm,1}$ admit a compact representation in terms of derivatives of Legendre polynomials (as for Remark 1, see [31, Eq. 4 and Sect. 3]). Let

$$B_{lm} = (-1)^{\left\lfloor \frac{l-m+1}{2} \right\rfloor} \frac{(l-1)!}{2^{l-1}\left(\frac{l-1}{2}\right)!\left(\frac{l+1}{2}\right)!}.$$

For $1 \le m \le l$, and odd l, we obtain

$$\begin{aligned} f^{+}_{lm,1} &= mB_{lm}S_I^{m-1}R_{lm}, \\ f^{-}_{lm,1} &= B_{lm}S_I^{m-1}\left(mC_IR_{lm} - S_I^2R'_{lm}\right), \end{aligned}$$

where S_I, C_I, and R_{lm} are defined in Eqs. (14). For the zonal case $m = 0$, these expressions simplify to

$$f^{+}_{l0,1} = 0, \qquad f^{-}_{l0,1} = -B_{l0}S_IP'_l.$$

3.3 The linear system for $\dot{\boldsymbol{\xi}}$, $\dot{\boldsymbol{\eta}}$

By adding the contributions given in Eqs. (12), (13) and (18), (19) of each even and odd harmonic up to the maximum degree $l_{\max}$, we obtain the following system:

$$\begin{cases} \dot{\xi} = K(t)\xi + K_\xi(t)\eta + C_\xi(t), \\ \dot{\eta} = -K(t)\eta + K_\eta(t)\xi + C_\eta(t), \end{cases} \tag{20}$$

where

$$K(t) = -\sum_{\substack{l=2 \\ \text{even}}}^{l_{\max}} \sum_{m=0}^{l} n\left(\frac{R_{\leftmoon}}{a}\right)^l M^{-}_{lm,2}(I)\tilde{\mathcal{S}}_{lm}(t), \tag{21}$$

$$K_\xi(t) = \sum_{\substack{l=2 \\ \text{even}}}^{l_{\max}} \sum_{m=0}^{l} n\left(\frac{R_{\leftmoon}}{a}\right)^l \left(M^{+}_{lm,2}(I) + N_{lm}(I)\right)\mathcal{S}_{lm}(t), \tag{22}$$

$$K_\eta(t) = \sum_{\substack{l=2 \\ \text{even}}}^{l_{\max}} \sum_{m=0}^{l} n\left(\frac{R_{\leftmoon}}{a}\right)^l \left(M^{+}_{lm,2}(I) - N_{lm}(I)\right)\mathcal{S}_{lm}(t), \tag{23}$$

$$C_\xi(t) = -\sum_{\substack{l=3 \\ \text{odd}}}^{l_{\max}} \sum_{m=0}^{l} n\left(\frac{R_{\leftmoon}}{a}\right)^l M^{-}_{lm,1}(I)\mathcal{S}^{*}_{lm}(t), \tag{24}$$

$$C_\eta(t) = \sum_{\substack{l=3\\ \text{odd}}}^{l_{\max}} \sum_{m=0}^{l} n \left(\frac{R_{\leftmoon}}{a}\right)^l M^+_{lm,1}(I)\tilde{\mathcal{S}}^*_{lm}(t). \tag{25}$$

The dependence on time arises through the variables Ω and θ. Indeed, we assume that

$$\Omega(t) = \Omega_0 + h_{\text{sec}}(t - t_0), \tag{26}$$
$$\theta(t) = \theta_0 + \omega_{\leftmoon}\,(t - t_0), \tag{27}$$

where h_{sec} is constant and depends on the mean values of a, e, I at the initial epoch t_0 as shown by Eq. (10) and $\omega_{\leftmoon}$ is the frequency of revolution of the Moon, i.e. $2\pi/T_{\leftmoon}$, with $T_{\leftmoon} = 27.321661$ days the sidereal month.

The coefficients K, K_ξ, and K_η come from the contributions of even harmonics, while C_ξ and C_η originate from those of odd harmonics. K_ξ, K_η, C_ξ are given by the sum of a constant term due to the zonal harmonics ($m = 0$) and an oscillatory term due to the non-zonal (sectorial and tesseral) harmonics:

$$K_\xi(t) = k_\xi + \hat{k}_\xi(t),$$
$$K_\eta(t) = k_\eta + \hat{k}_\eta(t),$$
$$C_\xi(t) = c_\xi + \hat{c}_\xi(t),$$

where

$$k_\xi = \sum_{\substack{l=2\\ \text{even}}}^{l_{\max}} n \left(\frac{R_{\leftmoon}}{a}\right)^l J_l\big(M^+_{l0,2}(I) + N_{l0}(I)\big), \tag{28}$$

$$k_\eta = \sum_{\substack{l=2\\ \text{even}}}^{l_{\max}} n \left(\frac{R_{\leftmoon}}{a}\right)^l J_l\big(M^+_{l0,2}(I) - N_{l0}(I)\big), \tag{29}$$

$$c_\xi = -\sum_{\substack{l=3\\ \text{odd}}}^{l_{\max}} n \left(\frac{R_{\leftmoon}}{a}\right)^l J_l M^-_{l0,1}(I), \tag{30}$$

with $J_l := C_{l0}$ denoting the zonal harmonic of degree l. Instead, the constant terms of K and C_η are equal to zero[3]. Note that, if only the zonal terms are retained, (20) reduces to the system considered by R.A. Cook [23]:

$$\begin{cases} \dot{\xi} = k_\xi \eta + c_\xi, \\ \dot{\eta} = k_\eta \xi. \end{cases} \tag{31}$$

The constant zonal coefficients k_ξ and k_η determine the reference coupling between ξ and η and govern their long-period evolution. The non-zonal components $K(t)$,

[3]Since $S_{l0} = 0$, we have $\tilde{\mathcal{S}}_{l0} = 0$, $\tilde{\mathcal{S}}^*_{l0} = 0$.

$\hat{k}_\xi(t)$, and $\hat{k}_\eta(t)$ modulate this coupling on intermediate timescales, with characteristic periods of the order of $T_{\mathbb{Q}}/m$. Motivated by the separation between these periods and the timescale of the reference dynamics, we assume that this oscillatory modulation has a negligible cumulative effect over the time intervals considered. Accordingly, we replace $K(t)$, $K_\xi(t)$, and $K_\eta(t)$ by 0, k_ξ, and k_η, respectively, in the system (20). The accuracy and limitations of this approximation are assessed numerically in Section 5, where the configurations in which the neglected terms become significant are also identified and discussed. On the other hand, the terms $C_\xi(t)$ and $C_\eta(t)$ directly force the eccentricity vector. We retain both their constant and oscillatory components to capture the corresponding forced response. In particular, a periodic forcing with zero temporal mean can still generate appreciable oscillations of the eccentricity vector. Our approximation thus preserves the full time dependence of the forcing terms while replacing the coupling coefficients by their constant zonal components.[4]

After applying the assumptions on the coefficients described above, (20) takes the form

$$\begin{cases} \dot{\xi} = k_\xi \eta + C_\xi(t), \\ \dot{\eta} = k_\eta \xi + C_\eta(t), \end{cases} \tag{32}$$

where $C_\xi(t)$, $C_\eta(t)$ are reported in Eqs. (24), (25) and k_ξ, k_η are obtained by retaining only the terms with $m = 0$ in $K_\xi(t)$, $K_\eta(t)$ (see Eqs. 28, 29). A comparison of systems (31) and (32) shows that our formulation extends that of R.A. Cook [23] by including the time-dependent forcing due to odd-degree non-zonal harmonics, which makes the system nonautonomous.

4 Analytical solution

Here, we derive the general solution of the system of differential equations (32). Applying the method of variation of parameters [32, Cap. 4, Eq. 4.45], the general solution can be written as

$$\begin{pmatrix} \xi(t) \\ \eta(t) \end{pmatrix} = \Phi(t, t_0) \begin{pmatrix} \xi_0 \\ \eta_0 \end{pmatrix} + \int_{t_0}^{t} \Phi(t, \tau) \begin{pmatrix} C_\xi(\tau) \\ C_\eta(\tau) \end{pmatrix} d\tau, \tag{33}$$

where $\Phi(t, t_0)$ is the state transition matrix of the homogeneous system

$$\begin{cases} \dot{\xi} = k_\xi \eta, \\ \dot{\eta} = k_\eta \xi \end{cases} \tag{34}$$

and $\xi_0 = \xi(t_0)$, $\eta_0 = \eta(t_0)$. The form of the solution of (34) depends on the eigenvalues $\pm\sqrt{k_\xi k_\eta}$ of the associated matrix. Let us introduce the quantity

$$\sigma = \sqrt{|k_\xi k_\eta|}.$$

[4] The singularity affecting $K_\xi(t)$ and $K_\eta(t)$ for $m = 1$, see Remark 2, is avoided because we keep only the zonal terms ($m = 0$) of these functions.

If $k_\xi k_\eta < 0$ the eigenvalues are imaginary and the solution is bounded and periodic. It results

$$\Phi(t,t_0) = \begin{pmatrix} \cos\left(\sigma(t-t_0)\right) & -\dfrac{\sigma}{k_\eta}\sin\left(\sigma(t-t_0)\right) \\ -\dfrac{\sigma}{k_\xi}\sin\left(\sigma(t-t_0)\right) & \cos\left(\sigma(t-t_0)\right) \end{pmatrix}, \tag{35}$$

where σ is the frequency of the long-period evolution, which is determined by the even zonal harmonics.

If $k_\xi k_\eta > 0$, the eigenvalues are real, and the solution exhibits hyperbolic behavior. In this case, we have

$$\Phi(t,t_0) = \begin{pmatrix} \cosh\left(\sigma(t-t_0)\right) & \dfrac{\sigma}{k_\eta}\sinh\left(\sigma(t-t_0)\right) \\ \dfrac{\sigma}{k_\xi}\sinh\left(\sigma(t-t_0)\right) & \cosh\left(\sigma(t-t_0)\right) \end{pmatrix}. \tag{36}$$

It should be noted that this solution is valid only within the linear regime. As the eccentricity increases the real evolution of the eccentricity vector can deviate significantly from the model's prediction [23]. In the eLLO regime, however, given the short lifetimes typical of these very low-altitude orbits, impact generally occurs before the eccentricity has time to grow enough to depart from the linear regime.

If $k_\xi k_\eta = 0$, then we obtain a zero eigenvalue with algebraic multiplicity two. For $l_{\max} = 2$ or 3, both coefficients vanish at the classical *critical* inclinations, $I = \arccos\left(1/\sqrt{5}\right)$ and $I = \pi - \arccos\left(1/\sqrt{5}\right)$. Then, the state transition matrix is the identity and the solution of the zonal problem is an equilibrium: both the mean eccentricity and the argument of perilune are *frozen*. In the cases $k_\xi = 0$, $k_\eta \neq 0$ and $k_\xi \neq 0$, $k_\eta = 0$, respectively, the state transition matrices are

$$\Phi(t,t_0) = \begin{pmatrix} 1 & 0 \\ k_\eta(t-t_0) & 1 \end{pmatrix}, \qquad \Phi(t,t_0) = \begin{pmatrix} 1 & k_\xi(t-t_0) \\ 0 & 1 \end{pmatrix}. \tag{37}$$

The homogeneous solution therefore exhibits linear growth for generic initial conditions.

The sign of the product $k_\xi k_\eta$ depends on the values of the mean semi-major axis and orbital inclination, as shown in Figure 1 for a range of altitudes relevant to this study. The map exhibits two main bands of hyperbolic behavior, one at prograde inclinations and its retrograde counterpart, which persist throughout the range of semi-major axes shown. The pattern is symmetric about $I = 90°$. At the smallest semi-major axes, two additional pairs of narrow regions appear between the main bands and the polar configuration. Their widths in inclination decrease as the semi-major axis increases, and the pair closest to $I = 90°$ disappears first. At larger semi-major axes, only the two main bands remain. For example, assuming $R_{\leftmoon} = 1738$ km and a mean semi-major axis of $R_{\leftmoon} + 20$ km we find that $k_\xi k_\eta > 0$ inside the prograde intervals $55.63° < I < 59.27°$, $62.17° < I < 64.57°$, $77.34° < I < 79.34°$.[5]

[5]The inclination intervals are reported using outward rounding to two decimal places: lower endpoints are rounded down and upper endpoints are rounded up. Thus, each unrounded lower endpoint lies less than

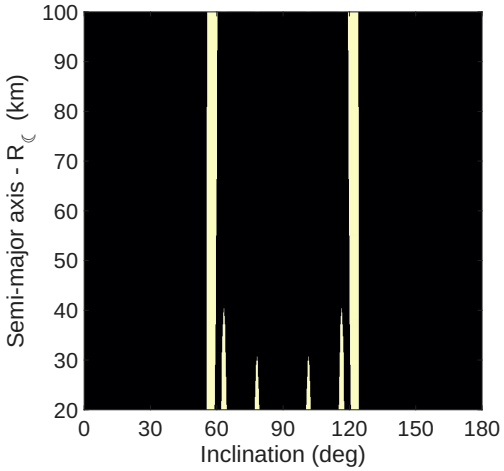


Fig. 1: Behavior of the mean eccentricity vector: periodic (black region), hyperbolic (light region) solution. This plot is obtained with $l_{\max} = 50$.

Let us introduce

$$\nu = \omega_{☾} - h_{\sec},$$

and

$$\gamma_0 = \Omega_0 - \theta_0 + \nu t_0, \qquad \delta_0 = \sigma t_0, \qquad \beta_0 = \nu t_0 - \gamma_0. \tag{38}$$

From Eqs. (26), (27), we have

$$\Omega(t) - \theta(t) = -(\nu t - \gamma_0),$$
$$\sigma(t - t_0) = \sigma t - \delta_0.$$

In view of the computation of the integral in Eq. (33), the forcing terms $\hat{c}_\xi(t)$ (see Eq. 30), $C_\eta(t)$ are written as

$$\hat{c}_\xi(t) = \sum_{\substack{l=3 \\ \text{odd}}}^{l_{\max}} \sum_{m=1}^{l} \left[A^\xi_{lm} \cos(m(\nu t - \gamma_0)) - B^\xi_{lm} \sin(m(\nu t - \gamma_0)) \right],$$

$$C_\eta(t) = \sum_{\substack{l=3 \\ \text{odd}}}^{l_{\max}} \sum_{m=1}^{l} \left[A^\eta_{lm} \cos(m(\nu t - \gamma_0)) - B^\eta_{lm} \sin(m(\nu t - \gamma_0)) \right],$$

where

$$A^\xi_{lm} = -n \left(\frac{R_{☾}}{a} \right)^l M^-_{lm,1}(I) \begin{pmatrix} C_{lm} \\ S_{lm} \end{pmatrix}^{m \text{ even}}_{m \text{ odd}},$$

0.01° above its reported value, while each unrounded upper endpoint lies less than 0.01° below its reported value.

$$B^{\xi}_{lm} = -n\left(\frac{R_{\leftmoon}}{a}\right)^{l} M^{-}_{lm,1}(I) \begin{pmatrix} S_{lm} \\ -C_{lm} \end{pmatrix}^{m\ \text{even}}_{m\ \text{odd}},$$
$$A^{\eta}_{lm} = n\left(\frac{R_{\leftmoon}}{a}\right)^{l} M^{+}_{lm,1}(I) \begin{pmatrix} -S_{lm} \\ C_{lm} \end{pmatrix}^{m\ \text{even}}_{m\ \text{odd}},$$
$$B^{\eta}_{lm} = n\left(\frac{R_{\leftmoon}}{a}\right)^{l} M^{+}_{lm,1}(I) \begin{pmatrix} C_{lm} \\ S_{lm} \end{pmatrix}^{m\ \text{even}}_{m\ \text{odd}}.$$

The general solution of Eq. (32) is provided below for the three cases $k_\xi k_\eta < 0$, $k_\xi k_\eta > 0$, $k_\xi k_\eta = 0$.

4.1 Solution for $k_\xi k_\eta < 0$

The solution is given by

$$\xi(t) = \xi_{\text{zon}}(t) + X_\sigma \cos(\sigma t - \delta_0) + Y_\sigma \sin(\sigma t - \delta_0) + \sum_{\substack{l=3 \\ \text{odd}}}^{l_{\max}} \sum_{m=1}^{l} \left[X_{\nu,lm} \cos(m(\nu t - \gamma_0)) + Y_{\nu,lm} \sin(m(\nu t - \gamma_0))\right], \tag{39}$$

$$\eta(t) = \eta_{\text{zon}}(t) + H_\sigma \cos(\sigma t - \delta_0) + J_\sigma \sin(\sigma t - \delta_0) + \sum_{\substack{l=3 \\ \text{odd}}}^{l_{\max}} \sum_{m=1}^{l} \left[H_{\nu,lm} \cos(m(\nu t - \gamma_0)) + J_{\nu,lm} \sin(m(\nu t - \gamma_0))\right], \tag{40}$$

where $\xi_{\text{zon}}(t)$, $\eta_{\text{zon}}(t)$ is the solution that we would obtain by considering only the zonal harmonics [see 23, Eqs. (41), (42)]:

$$\xi_{\text{zon}}(t) = \xi_0 \cos(\sigma t - \delta_0) + \left(\frac{c_\xi}{\sigma} - \frac{\sigma}{k_\eta}\eta_0\right) \sin(\sigma t - \delta_0),$$
$$\eta_{\text{zon}}(t) = -\frac{c_\xi}{k_\xi} + \left(\eta_0 + \frac{c_\xi}{k_\xi}\right) \cos(\sigma t - \delta_0) - \frac{\sigma}{k_\xi}\xi_0 \sin(\sigma t - \delta_0).$$

Moreover, we have

$$X_\sigma = \sum_{\substack{l=3 \\ \text{odd}}}^{l_{\max}} \sum_{m=1}^{l} \frac{1}{\sigma^2 - m^2\nu^2} \left[a^{\xi}_{lm} \cos(m\beta_0) + b^{\xi}_{lm} \sin(m\beta_0)\right],$$

$$Y_\sigma = \sum_{\substack{l=3 \\ \text{odd}}}^{l_{\max}} \sum_{m=1}^{l} \frac{\sigma}{\sigma^2 - m^2\nu^2} \left[c^{\xi}_{lm} \cos(m\beta_0) - d^{\xi}_{lm} \sin(m\beta_0)\right],$$

$$X_{\nu,lm} = -\frac{a^{\xi}_{lm}}{\sigma^2 - m^2\nu^2}, \qquad Y_{\nu,lm} = -\frac{b^{\xi}_{lm}}{\sigma^2 - m^2\nu^2},$$

and

$$H_\sigma = \sum_{\substack{l=3\\ \text{odd}}}^{l_{\max}} \sum_{m=1}^{l} \frac{1}{\sigma^2 - m^2\nu^2} \left[a^\eta_{lm} \cos(m\beta_0) + b^\eta_{lm} \sin(m\beta_0)\right],$$

$$J_\sigma = \sum_{\substack{l=3\\ \text{odd}}}^{l_{\max}} \sum_{m=1}^{l} \frac{\sigma}{\sigma^2 - m^2\nu^2} \left[c^\eta_{lm} \cos(m\beta_0) - d^\eta_{lm} \sin(m\beta_0)\right],$$

$$H_{\nu,lm} = -\frac{a^\eta_{lm}}{\sigma^2 - m^2\nu^2}, \qquad J_{\nu,lm} = -\frac{b^\eta_{lm}}{\sigma^2 - m^2\nu^2},$$

with

$$a^\xi_{lm} = m\nu B^\xi_{lm} + \frac{\sigma^2}{k_\eta} A^\eta_{lm}, \qquad b^\xi_{lm} = m\nu A^\xi_{lm} - \frac{\sigma^2}{k_\eta} B^\eta_{lm}, \tag{41}$$

$$c^\xi_{lm} = A^\xi_{lm} - \frac{m\nu}{k_\eta} B^\eta_{lm}, \qquad d^\xi_{lm} = B^\xi_{lm} + \frac{m\nu}{k_\eta} A^\eta_{lm}, \tag{42}$$

$$a^\eta_{lm} = m\nu B^\eta_{lm} + \frac{\sigma^2}{k_\xi} A^\xi_{lm}, \qquad b^\eta_{lm} = m\nu A^\eta_{lm} - \frac{\sigma^2}{k_\xi} B^\xi_{lm}, \tag{43}$$

$$c^\eta_{lm} = A^\eta_{lm} - \frac{m\nu}{k_\xi} B^\xi_{lm}, \qquad d^\eta_{lm} = B^\eta_{lm} + \frac{m\nu}{k_\xi} A^\xi_{lm}. \tag{44}$$

The denominator $\sigma^2 - m^2\nu^2$ is equal to 0 if $\sigma = m\nu$. However, $\sigma^2 - m^2\nu^2 \neq 0$ in the domain $\mathcal{D} = \{(I, a) : 20 \text{ km} \leq a - R_{\leftmoon} \leq 100 \text{ km}, 0 \leq I \leq \pi\}$ (see Fig. 1) since for $l_{\max} = 50$ we have $\nu \approx \omega_{\leftmoon} \approx 10 \max_{\mathcal{D}} |\sigma|$.

4.2 Solution for $k_\xi k_\eta > 0$

The solution is given by

$$\begin{aligned}\xi(t) = \xi_{\text{zon}}(t) &+ \hat{X}_\sigma \cosh(\sigma t - \delta_0) + \hat{Y}_\sigma \sinh(\sigma t - \delta_0) \\ &+ \sum_{\substack{l=3\\ \text{odd}}}^{l_{\max}} \sum_{m=1}^{l} \left[\hat{X}_{\nu,lm} \cos(m(\nu t - \gamma_0)) + \hat{Y}_{\nu,lm} \sin(m(\nu t - \gamma_0))\right],\end{aligned}$$

$$\begin{aligned}\eta(t) = \eta_{\text{zon}}(t) &+ \hat{H}_\sigma \cosh(\sigma t - \delta_0) + \hat{J}_\sigma \sinh(\sigma t - \delta_0) \\ &+ \sum_{\substack{l=3\\ \text{odd}}}^{l_{\max}} \sum_{m=1}^{l} \left[\hat{H}_{\nu,lm} \cos(m(\nu t - \gamma_0)) + \hat{J}_{\nu,lm} \sin(m(\nu t - \gamma_0))\right],\end{aligned}$$

where $\xi_{\text{zon}}(t)$, $\eta_{\text{zon}}(t)$ is the solution that we would obtain by considering only the zonal harmonics [see 23, Eqs. (41), (42)]:

$$\xi_{\text{zon}}(t) = \xi_0 \cosh(\sigma t - \delta_0) + \left(\frac{\sigma}{k_\eta}\eta_0 + \frac{c_\xi}{\sigma}\right)\sinh(\sigma t - \delta_0),$$
$$\eta_{\text{zon}}(t) = -\frac{c_\xi}{k_\xi} + \left(\eta_0 + \frac{c_\xi}{k_\xi}\right)\cosh(\sigma t - \delta_0) + \frac{\sigma}{k_\xi}\xi_0 \sinh(\sigma t - \delta_0).$$

Moreover, we have

$$\hat{X}_\sigma = \sum_{\substack{l=3\\ \text{odd}}}^{l_{\max}} \sum_{m=1}^{l} \frac{1}{\sigma^2 + m^2\nu^2}\left[\hat{a}^\xi_{lm}\cos(m\beta_0) - \hat{b}^\xi_{lm}\sin(m\beta_0)\right],$$

$$\hat{Y}_\sigma = \sum_{\substack{l=3\\ \text{odd}}}^{l_{\max}} \sum_{m=1}^{l} \frac{\sigma}{\sigma^2 + m^2\nu^2}\left[c^\xi_{lm}\cos(m\beta_0) - d^\xi_{lm}\sin(m\beta_0)\right],$$

$$\hat{X}_{\nu,lm} = -\frac{\hat{a}^\xi_{lm}}{\sigma^2 + m^2\nu^2}, \qquad \hat{Y}_{\nu,lm} = \frac{\hat{b}^\xi_{lm}}{\sigma^2 + m^2\nu^2},$$

and

$$\hat{H}_\sigma = \sum_{\substack{l=3\\ \text{odd}}}^{l_{\max}} \sum_{m=1}^{l} \frac{1}{\sigma^2 + m^2\nu^2}\left[\hat{a}^\eta_{lm}\cos(m\beta_0) - \hat{b}^\eta_{lm}\sin(m\beta_0)\right],$$

$$\hat{J}_\sigma = \sum_{\substack{l=3\\ \text{odd}}}^{l_{\max}} \sum_{m=1}^{l} \frac{\sigma}{\sigma^2 + m^2\nu^2}\left[c^\eta_{lm}\cos(m\beta_0) - d^\eta_{lm}\sin(m\beta_0)\right],$$

$$\hat{H}_{\nu,lm} = -\frac{\hat{a}^\eta_{lm}}{\sigma^2 + m^2\nu^2}, \qquad \hat{J}_{\nu,lm} = \frac{\hat{b}^\eta_{lm}}{\sigma^2 + m^2\nu^2},$$

with (c^ξ_{lm}, d^ξ_{lm}) given in Eqs. (42), $(c^\eta_{lm}, d^\eta_{lm})$ in Eqs. (44) and

$$\hat{a}^\xi_{lm} = -m\nu B^\xi_{lm} + \frac{\sigma^2}{k_\eta}A^\eta_{lm}, \qquad \hat{b}^\xi_{lm} = m\nu A^\xi_{lm} + \frac{\sigma^2}{k_\eta}B^\eta_{lm},$$
$$\hat{a}^\eta_{lm} = -m\nu B^\eta_{lm} + \frac{\sigma^2}{k_\xi}A^\xi_{lm}, \qquad \hat{b}^\eta_{lm} = m\nu A^\eta_{lm} + \frac{\sigma^2}{k_\xi}B^\xi_{lm}.$$

4.3 Solution for $k_\xi k_\eta = 0$

If $k_\xi = 0$, $k_\eta \neq 0$ the solution is

$$\xi(t) = \xi_{\rm zon}(t) + H^\xi + \sum_{\substack{l=3\\ \rm odd}}^{l_{\max}} \sum_{m=1}^{l} \frac{1}{m\nu} \left[B^\xi_{lm} \cos(m(\nu t - \gamma_0)) + A^\xi_{lm} \sin(m(\nu t - \gamma_0)) \right],$$

$$\eta(t) = \eta_{\rm zon}(t) + J^\eta + k_\eta H^\xi (t - t_0) + \sum_{\substack{l=3\\ \rm odd}}^{l_{\max}} \sum_{m=1}^{l} \frac{1}{m\nu} \left[e^\eta_{lm} \cos(m(\nu t - \gamma_0)) + f^\eta_{lm} \sin(m(\nu t - \gamma_0)) \right], \tag{45}$$

where

$$\xi_{\rm zon}(t) = \xi_0 + c_\xi (t - t_0), \tag{46}$$
$$\eta_{\rm zon}(t) = \eta_0 + \xi_0 k_\eta (t - t_0) + \frac{k_\eta c_\xi}{2} (t - t_0)^2$$

and

$$H^\xi = -\sum_{\substack{l=3\\ \rm odd}}^{l_{\max}} \sum_{m=1}^{l} \frac{1}{m\nu} \left[B^\xi_{lm} \cos(m\beta_0) + A^\xi_{lm} \sin(m\beta_0) \right], \tag{47}$$
$$J^\eta = -\sum_{\substack{l=3\\ \rm odd}}^{l_{\max}} \sum_{m=1}^{l} \frac{1}{m\nu} \left[e^\eta_{lm} \cos(m\beta_0) + f^\eta_{lm} \sin(m\beta_0) \right],$$
$$e^\eta_{lm} = B^\eta_{lm} - \frac{k_\eta}{m\nu} A^\xi_{lm}, \qquad f^\eta_{lm} = A^\eta_{lm} + \frac{k_\eta}{m\nu} B^\xi_{lm}.$$

If $k_\eta = 0$, $k_\xi \neq 0$ the solution is

$$\xi(t) = \xi_{\rm zon}(t) + J^\xi + k_\xi H^\eta (t - t_0) + \sum_{\substack{l=3\\ \rm odd}}^{l_{\max}} \sum_{m=1}^{l} \frac{1}{m\nu} \left[e^\xi_{lm} \cos(m(\nu t - \gamma_0)) + f^\xi_{lm} \sin(m(\nu t - \gamma_0)) \right],$$

$$\eta(t) = \eta_{\rm zon}(t) + H^\eta + \sum_{\substack{l=3\\ \rm odd}}^{l_{\max}} \sum_{m=1}^{l} \frac{1}{m\nu} \left[B^\eta_{lm} \cos(m(\nu t - \gamma_0)) + A^\eta_{lm} \sin(m(\nu t - \gamma_0)) \right], \tag{48}$$

where

$$\xi_{\rm zon}(t) = \xi_0 + (\eta_0 k_\xi + c_\xi)(t - t_0),$$

$$\eta_{\mathrm{zon}}(t) = \eta_0 \tag{49}$$

and

$$H^{\eta} = -\sum_{\substack{l=3\\ \text{odd}}}^{l_{\max}} \sum_{m=1}^{l} \frac{1}{m\nu} \left[B^{\eta}_{lm} \cos(m\beta_0) + A^{\eta}_{lm} \sin(m\beta_0) \right], \tag{50}$$

$$J^{\xi} = -\sum_{\substack{l=3\\ \text{odd}}}^{l_{\max}} \sum_{m=1}^{l} \frac{1}{m\nu} \left[e^{\xi}_{lm} \cos(m\beta_0) + f^{\xi}_{lm} \sin(m\beta_0) \right],$$

$$e^{\xi}_{lm} = B^{\xi}_{lm} - \frac{k_{\xi}}{m\nu} A^{\eta}_{lm}, \qquad f^{\xi}_{lm} = A^{\xi}_{lm} + \frac{k_{\xi}}{m\nu} B^{\eta}_{lm}.$$

Finally, the condition $k_{\xi} = k_{\eta} = 0$ can be satisfied only if $l_{\max} = 2, 3$. For $l_{\max} = 3$, the solution $\xi(t)$ is given by Eqs. (45), (46), (47) and the solution $\eta(t)$ is given by Eqs. (48), (49), (50). For $l_{\max} = 2$, we have an equilibrium: $\xi(t) = \xi_0$, $\eta(t) = \eta_0$.

5 Model validation and results

This section presents a detailed validation of the proposed analytical model by comparing its predictions with numerical propagations over a grid of initial conditions. The first objective is to identify the regions in which the assumptions underlying the theory provide an adequate approximation. The second is to assess how accurately the model reproduces the main long- and medium-period features of the eccentricity evolution within those regions.

The numerical reference propagations are performed with the Orekit library [33], using a lunar spherical-harmonic gravity field truncated at degree and order 50, together with the third-body perturbations of the Earth and the Sun. Each reference trajectory is propagated for 365 days or until impact with the lunar surface, whichever occurs first. In all tests presented in this section, the initial osculating angular elements are set to $\omega_0 = \Omega_0 = M_0 = 0°$. Following the map-based validation strategy adopted by Mastroianni et al. [15], we consider a grid of initial inclination and eccentricity. Specifically, 100 inclination values are sampled uniformly over $[0°, 90°]$, and 100 initial eccentricities are considered from zero up to $0.7(1 - R_{\leftmoon}/a_0)$. Here, $1 - R_{\leftmoon}/a_0$ is the eccentricity corresponding to a perilune radius equal to $R_{\leftmoon}$ at the prescribed initial semi-major axis a_0. The analysis is repeated for $a_0 = R_{\leftmoon} + h$, with $h = 25$, 50, and 75 km. The primary validation metric is the maximum absolute eccentricity difference over the comparison interval,

$$\Delta e_{\max} = \max_{t \in [t_0, t_f]} |e_{\mathrm{a}}(t) - e_{\mathrm{n}}(t)|, \tag{51}$$

where $e_{\mathrm{a}}(t)$ and $e_{\mathrm{n}}(t)$ denote the analytical and numerical eccentricities, respectively, and t_f is either $t_0 + 365$ days or the impact time of the numerical reference trajectory. The error maps display $\log_{10}(\Delta e_{\max})$ in order to better distinguish the accuracy levels across the tested domain.

The analytical formulation allows an arbitrary truncation of the lunar gravity field. For the present validation, the maximum degree and order are both set to 50, as in the numerical reference model. This common truncation avoids discrepancies caused by using different maximum degrees and orders. However, it does not make the two dynamical models equivalent: the analytical solution retains only the contributions specified in the preceding sections, subject to the averaging, eccentricity truncation, and additional approximations introduced there.

A practical issue concerns the initialization of the analytical solution. We estimate the mean initial conditions numerically from the reference trajectory over one orbital revolution centered at t_0. The averaging is performed on the variables a, $\xi = e\cos\omega$, $\eta = e\sin\omega$, $p = \tan(I/2)\sin\Omega$, and $q = \tan(I/2)\cos\Omega$. The initial mean elements used by the analytical solution are then reconstructed from these averaged quantities. This procedure provides numerical estimates of the mean initial conditions, rather than an exact transformation to the mean elements of the analytical theory.

The analytical solution describes mean elements, whereas the numerical reference trajectory is expressed in osculating elements. Accordingly, the error metric reflects both discrepancies in the evolution of the mean elements and the short-period variations absent from the analytical solution. Therefore, the comparison measures the ability of the reduced theory to approximate the numerical eccentricity evolution, while it does not isolate the error in the mean-element dynamics alone.

The global results are summarized in Figures 2–4 for altitudes of 25, 50, and 75 km. The maps indicate an overall tendency toward larger errors at higher altitudes, although this trend is not uniform across the tested domain. Comparatively small errors are more widespread in the 25 km map, whereas bands of larger errors become more pronounced at 50 and 75 km. Several effects may contribute to this trend. The initial eccentricity range increases with altitude, potentially making the truncation in eccentricity less accurate. Moreover, for trajectories that survive longer, small differences between the analytical and numerical oscillation frequencies may lead to increasing phase differences and hence larger eccentricity errors over the comparison interval. The error maps remain nearly unchanged when third-body perturbations are omitted from the numerical reference propagations. This suggests that, in the cases considered, the errors and their altitude dependence are primarily associated with the approximations underlying the analytical model, including those introduced in the treatment of lunar harmonics.

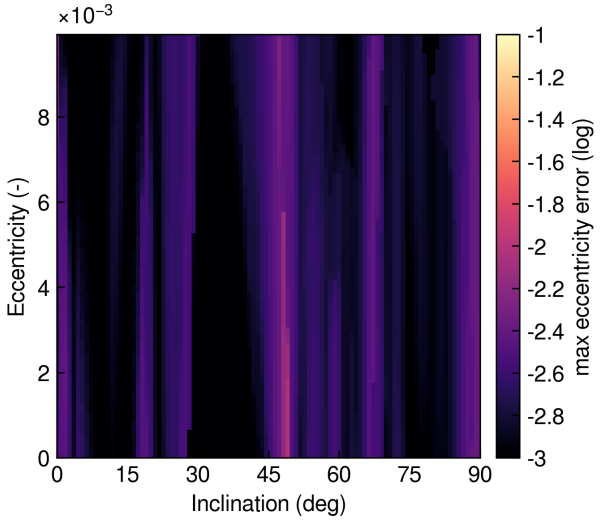


Fig. 2: Map of $\log_{10}(\Delta e_{\max})$ in the initial (osculating) eccentricity-inclination plane, with the remaining initial (osculating) conditions $a_0 = R_{☾} + 25$ km.

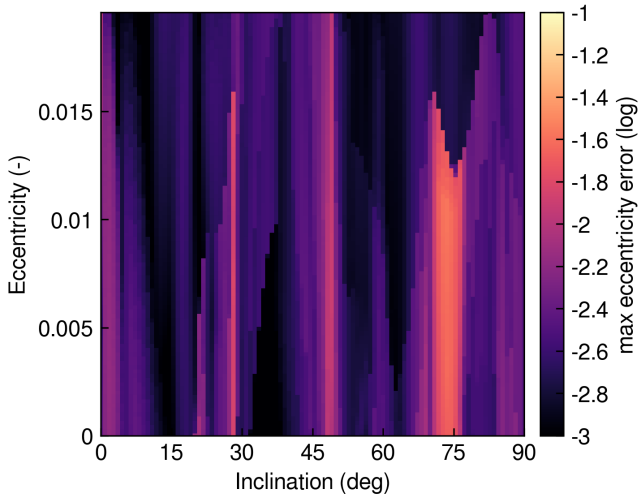


Fig. 3: Map of $\log_{10}(\Delta e_{\max})$ in the initial (osculating) eccentricity-inclination plane, with the remaining initial (osculating) conditions $a_0 = R_{☾} + 50$ km.

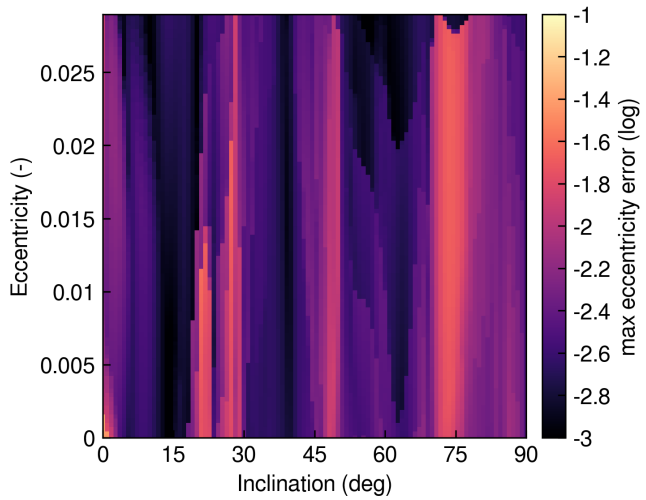


Fig. 4: Map of $\log_{10}(\Delta e_{\max})$ in the initial (osculating) eccentricity-inclination plane, with the remaining initial (osculating) conditions $a_0 = R_{\leftmoon} + 75$ km.

In addition to the altitude dependence, the maps show a pronounced variation of the error with inclination. Particularly at 25 km, comparatively small errors occur over several intervals of low and moderate inclination and extend across much of the tested eccentricity range. A band of larger errors near 49° is already visible at 25 km and becomes more pronounced in the 50 and 75 km maps. At 50 km, another prominent band appears near 27°–29°. At 75 km, this part of the map exhibits additional structure extending toward lower inclinations, particularly around 20°–23° at smaller initial eccentricities. At higher inclinations, a prominent band of larger errors spans approximately 70°–78° at 50 km and becomes broader at 75 km. The intensity and inclination extent of these features depend on the initial eccentricity.

Representative trajectories illustrating close agreement and large discrepancies are shown in Figures 5–8 and 10. Figure 5 presents a case at 25 km altitude within a region of small errors. The analytical solution captures the main eccentricity variations over the propagation interval. Although the numerical inclination oscillates and the nodal longitude departs from its prescribed linear evolution, the eccentricity remains in good agreement with the analytical prediction. This example shows that departures from the assumed orbital-plane evolution do not necessarily produce a large eccentricity error over the interval considered. Figure 6 presents two further examples at altitudes of 50 and 75 km, with numerical impact times of approximately 100 and 200 days, respectively. The analytical solution remains in good agreement with the numerical reference over these longer intervals, reproducing the main eccentricity oscillations and their overall evolution. These examples show that good agreement is not confined to the shortest-lived trajectories.

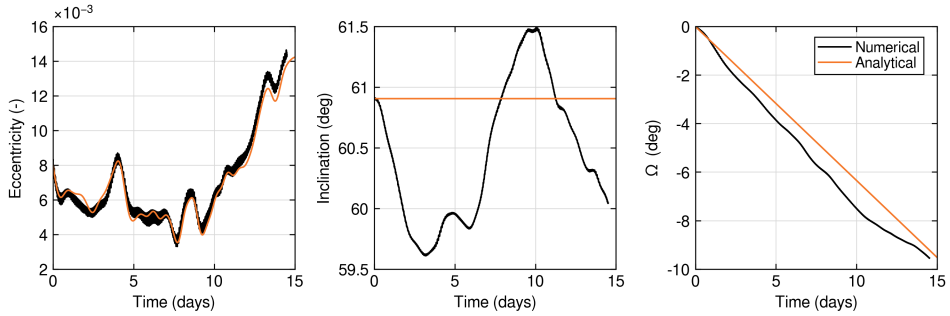


Fig. 5: Numerical and analytical evolution of the eccentricity, inclination, and longitude of the node for an orbit with initial (osculating) conditions $a_0 = R_{\leftmoon} + 25$ km, $e_0 = 0.0082$, $I_0 = 60.91°$.

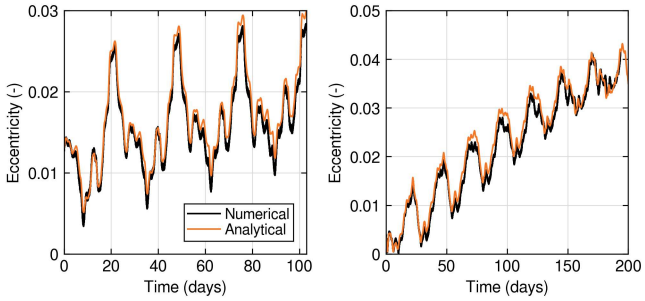


Fig. 6: Numerical and analytical evolution of the eccentricity for an orbit with initial (osculating) conditions: (left) $a_0 = R_{\leftmoon} + 50$ km, $e_0 = 0.0131$, $I_0 = 85.45°$; (right) $a_0 = R_{\leftmoon} + 75$ km, $e_0 = 0.0041$, $I_0 = 50.91°$.

Next, we examine the localized discrepancy near 49°. Figure 7 shows a trajectory at 25 km altitude for which the analytical and numerical eccentricities gradually separate in their slower modulation. The numerical trajectory impacts the lunar surface after approximately 120 days, limiting the interval over which this discrepancy can be followed. To examine its development over a longer interval, Figure 8 presents a case at 50 km altitude, with initial eccentricity $e_0 = 0.005736$, that survives throughout the 365 days propagation. The analytical and numerical solutions retain a similar medium-period structure, while their slower modulations differ. Figure 9 examines the role of omitted harmonics by comparing the full reference propagation with two reduced numerical models. The first retains all zonal harmonics and the odd-degree non-zonal harmonics up to degree 50. The second additionally includes the terms associated with C_{22}, S_{22}, C_{43}, and S_{43}. The reduced numerical models integrate the equations of motion directly and therefore do not reproduce all the approximations of the analytical solution. Adding these harmonics brings the slow eccentricity evolution

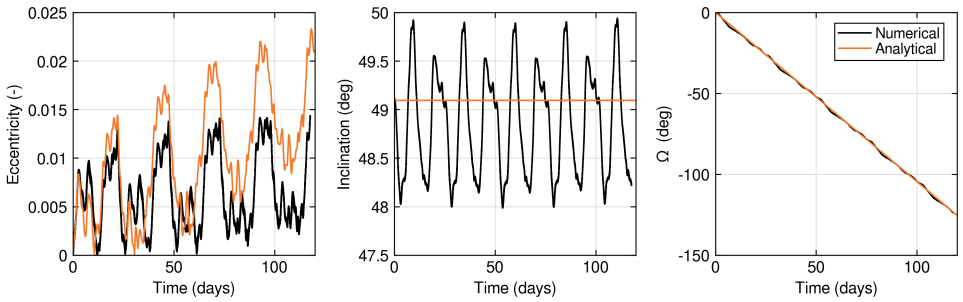


Fig. 7: Numerical and analytical evolution of the eccentricity, inclination, and longitude of the node for an orbit with initial (osculating) conditions $a_0 = R_{☾} + 25$ km, $e_0 = 0.0002$, $I_0 = 49.09°$.

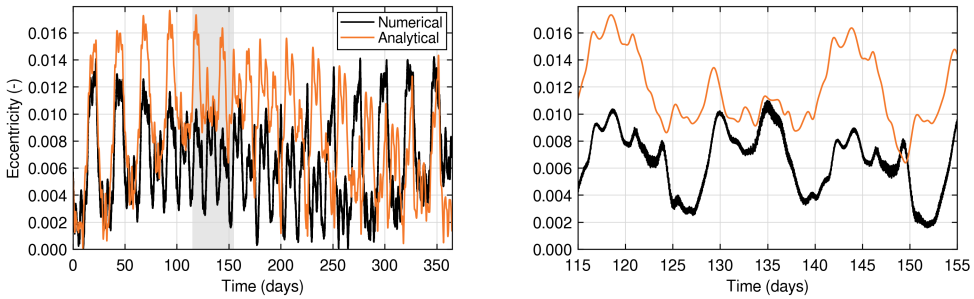


Fig. 8: Numerical and analytical evolution of the eccentricity for an orbit with initial (osculating) conditions $a_0 = R_{☾} + 50$ km, $e_0 = 0.005736$, $I_0 = 49°$. The left panel shows the full one-year propagation, while the right panel provides a close-up of the interval shaded in gray in the left panel, highlighting the discrepancy in the long-period modulation.

substantially closer to the full numerical result. This indicates that omitted even-degree non-zonal harmonics contribute appreciably to the discrepancy in this case. In particular, the oscillatory character of their contributions does not guarantee a negligible effect on the slow evolution over the comparison interval. However, adding the harmonics together does not identify their individual contributions, nor does it distinguish their direct effect on eccentricity from their effects through the evolution of the other orbital elements. A dedicated analysis would be required to explain their selective importance near this inclination.

Figure 10 presents a further case at 75 km altitude, with $I_0 = 73.64°$ and $e_0 = 0.008485$. Over the one-year propagation, the analytical solution develops a growing discrepancy in its slowly varying eccentricity level, with increasingly overestimated peaks. Figure 11 repeats the reduced-model comparison of Figure 9 for this case. Here, restoring the sectorial terms associated with C_{22} and S_{22} substantially improves

the agreement with the full numerical reference and largely removes the growing discrepancy. This provides a second example in which omitted even-degree non-zonal harmonics have a substantial effect on the eccentricity evolution.

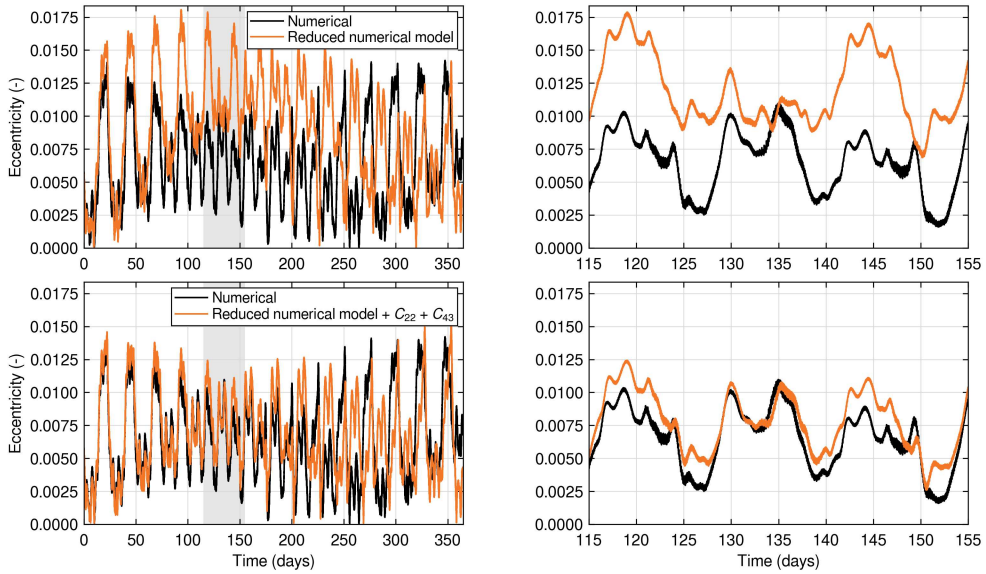


Fig. 9: Numerical evolution of the eccentricity for the same initial conditions as in Fig. 8. The upper panels compare the full numerical propagation with a reduced model retaining all zonal and odd-degree non-zonal harmonics. The lower panels show the same comparison after adding the terms associated with C_{22}, S_{22}, C_{43}, and S_{43} to the reduced model.

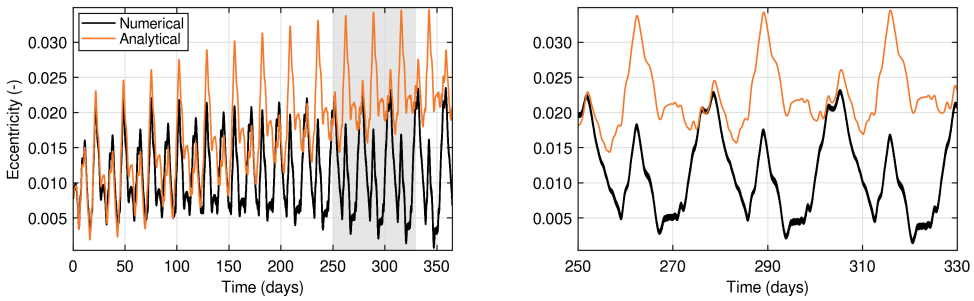


Fig. 10: Numerical and analytical evolution of the eccentricity for an orbit with initial (osculating) conditions $a_0 = R_{\leftmoon} + 75$ km, $e_0 = 0.008485$, $I_0 = 73.64°$. The left panel shows the full one-year propagation, while the right panel provides a close-up of the interval shaded in gray in the left panel, highlighting the discrepancy in the long-period modulation.

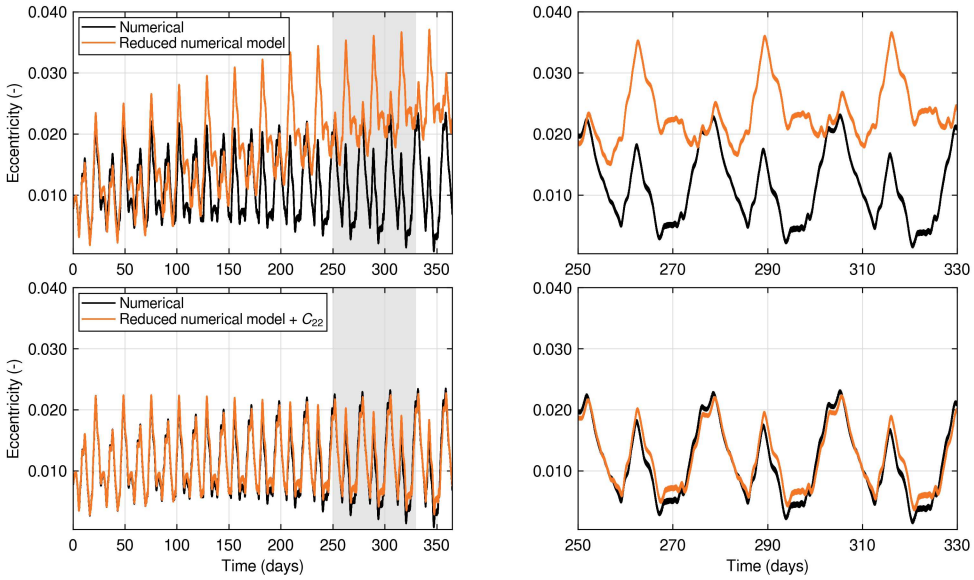


Fig. 11: Numerical evolution of the eccentricity for the same initial conditions as in Fig. 10. The upper panels compare the full numerical propagation with a reduced model retaining all zonal and odd-degree non-zonal harmonics. The lower panels show the same comparison after adding the terms associated with C_{22} and S_{22} to the reduced model.

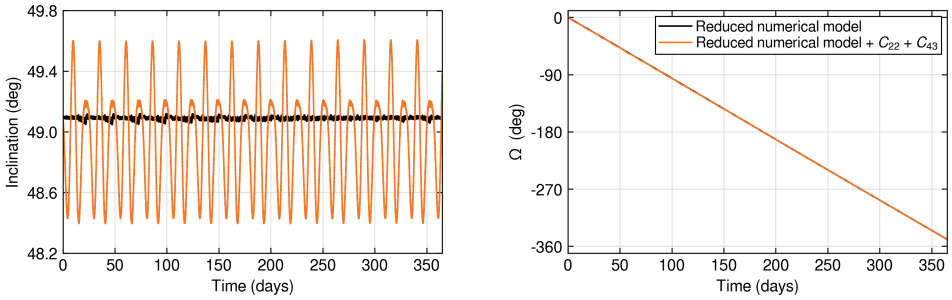


Fig. 12: Numerical evolution of the inclination (left) and longitude of the node (right) for the same initial conditions as in Fig. 8. The curves compare a reduced model retaining all zonal and odd-degree non-zonal harmonics with the same model augmented by the terms associated with C_{22}, S_{22}, C_{43}, and S_{43}.

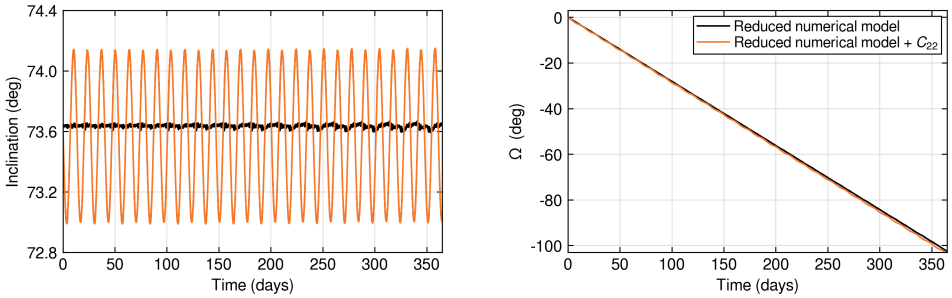


Fig. 13: Numerical evolution of the inclination (left) and longitude of the node (right) for the same initial conditions as in Fig. 10. The curves compare a reduced model retaining all zonal and odd-degree non-zonal harmonics with the same model augmented by the terms associated with C_{22} and S_{22}.

Further insight into these discrepancies is provided by Figures 12 and 13, which show the inclination and nodal longitude for the reduced numerical propagations considered in Figures 9 and 11, respectively. In both cases, the inclination remains nearly constant in the reduced model retaining only zonal and odd-degree non-zonal harmonics. Restoring the selected even-degree non-zonal harmonics introduces pronounced medium-period oscillations, with a peak-to-peak inclination variation of approximately one degree. The nodal curves, by contrast, remain close.

These results highlight a further consequence of omitting even-degree non-zonal harmonics. Besides contributing directly to the eccentricity equations, these harmonics modify the inclination, which enters both the coefficients of the homogeneous system and the odd-degree forcing terms. The constant inclination approximation therefore excludes an additional mechanism through which the omitted harmonics can affect the

eccentricity evolution. Taken together with the eccentricity comparisons in Figures 9 and 11, these results suggest that accounting for their influence on the inclination may be important for improving the analytical model.

The comparisons shown in this section characterize the performance of the analytical formulation for the initial conditions and propagation intervals considered here. Over substantial portions of the tested domain, the solution captures the main long- and medium-period features of the eccentricity evolution and can serve as a tool for interpreting the dynamics and rapidly exploring parameter dependence. Its accuracy is reduced in localized bands at intermediate and high inclinations. The numerical experiments near 49° and 73.64° identify selected omitted even-degree non-zonal harmonics as important contributors in those cases. Their effects and the roles of the other approximations underlying the model require further assessment. The solution may also remain useful over finite intervals in parts of the hyperbolic domain identified in Figure 1. At very low altitudes, impact can occur while the eccentricity is still small, limiting the time available for departures from the linear approximation to develop. Nevertheless, short lifetime alone does not guarantee accuracy, which must be assessed through comparison with the numerical reference. The applicability established by the present tests is also restricted to the sampled initial angular configurations.

6 Conclusions

This work has developed a compact first-order analytical model for the evolution of the mean eccentricity vector in near-circular eLLOs, extending the formulations of G.E. Cook and R.A. Cook by including the explicit forcing produced by odd-degree tesseral and sectorial harmonics. The resulting solution provides closed-form expressions for the evolution of the non-singular components ξ and η, while keeping the retained harmonic contributions explicit.

The numerical assessment compares the analytical solution with propagations including a 50×50 lunar gravity field and the third-body perturbations of the Earth and the Sun, over grids of initial eccentricity and inclination at altitudes of 25, 50, and 75 km. Each comparison extends over 365 days or until numerical impact, whichever occurs first. The results show that the solution reproduces the main long- and medium-period features of the eccentricity evolution over substantial portions of the tested domain, particularly at low and moderate inclinations and away from the localized discrepancy bands. In the regions of best agreement, $\Delta e_{\max}$ is of order 10^{-3} or smaller over the comparison interval. This error measure also includes the short-period variations absent from the mean-element solution. The validation is restricted to the sampled initial angular configuration, with $\omega_0 = \Omega_0 = M_0 = 0°$.

The validation also identifies limitations of the reduced theory. The maps generally show larger errors as altitude increases, although the sampled eccentricity ranges and comparison durations also change. Repeating the reference propagations without third-body perturbations produces nearly unchanged error maps, indicating that their omission is not a major source of error in the cases considered. Localized bands of larger error occur near 27°–29° and 49°, with additional structure extending toward lower inclinations at 75 km. A broader band spans approximately 70°–78° at 50 km

and becomes more extensive at 75 km. Errors in these regions can reach the 10^{-2} level. For the case examined near 49°, adding the terms associated with C_{22}, S_{22}, C_{43}, and S_{43} to a reduced numerical model substantially improves its agreement with the slow eccentricity evolution of the full numerical solution. For the case at 75 km with $I_0 = 73.64°$, restoring C_{22} and S_{22} alone similarly removes much of the growing discrepancy. These comparisons show that selected omitted even-degree non-zonal harmonics can contribute appreciably to the eccentricity evolution. The accompanying orbital-plane comparisons also reveal pronounced medium-period inclination oscillations when these harmonics are restored. Because inclination enters both the coefficients and the forcing terms of the eccentricity equations, these variations suggest an additional route through which the omitted harmonics may affect eccentricity, which the constant-inclination approximation cannot represent.

The solution can also remain practically useful over finite intervals in parts of the hyperbolic regime. At these very low altitudes, impact can occur while the eccentricity is still small, limiting the time available for departures from the linear approximation to develop. However, a short lifetime alone does not guarantee accuracy.

The present formulation provides a compact interpretative complement to high-fidelity numerical propagation for the long- and medium-period eccentricity dynamics within the regime where its assumptions remain applicable. Future work should address the limitations identified here, particularly through the inclusion of even-degree non-zonal harmonics, whose medium-period effects are included in the transformation of Knežević and Milani [12] for nearly polar orbits, and a more complete treatment of the inclination and nodal dynamics. A transformation between osculating and mean initial elements consistent with the analytical theory would also improve the initialization procedure. The localized discrepancy bands deserve further analytical study to clarify how specific neglected harmonics modify the long-period response and why the discrepancies are concentrated in these inclination ranges.

References

[1] Yarndley, J., Lara, M., Holt, H., Armellin, R.: Origins and application of the translation theorem in extremely low lunar orbits. Journal of Guidance, Control, and Dynamics **49**(3), 673–692 (2026)

[2] Konopliv, A.S., Sjogren, W.L., Wimberly, R.N., Cook, R.A., Vijayaraghavan, A.: A high resolution lunar gravity field and predicted orbit behavior. In: Astrodynamics 1993. Advances in the Astronautical Sciences, vol. 85, pp. 1275–1295. Univelt, San Diego, CA (1994). AAS Paper 93-622

[3] Roncoli, R.B.: Lunar constants and models document. Technical Report JPL D-32296, Jet Propulsion Laboratory, California Institute of Technology, Pasadena, CA (September 2005)

[4] Ramanan, R.V., Adimurthy, V.: An analysis of near-circular lunar mapping orbits. Journal of Earth System Science **114**(6), 619–626 (2005)

[5] Lara, M.: Design of long-lifetime lunar orbits: A hybrid approach. Acta Astronautica **69**(3–4), 186–199 (2011)

[6] Park, S.-Y., Junkins, J.L.: Orbital mission analysis for a lunar mapping satellite. In: Astrodynamics Conference, pp. 93–98. American Institute of Aeronautics and Astronautics, Scottsdale, AZ (1994). AIAA Paper 94-3717

[7] Meyer, K.W., Buglia, J.J., Desai, P.N.: Lifetimes of lunar satellite orbits. Technical Report NASA-TP-3394, NASA Langley Research Center, Hampton, VA (March 1994)

[8] Nie, T., Gurfil, P.: Lunar frozen orbits revisited. Celestial Mechanics and Dynamical Astronomy **130**(10), 61 (2018)

[9] Folta, D., Quinn, D.: Lunar frozen orbits. In: AIAA/AAS Astrodynamics Specialist Conference and Exhibit. American Institute of Aeronautics and Astronautics, Keystone, CO (2006). AIAA Paper 2006-6749

[10] Russell, R.P., Lara, M.: Long-lifetime lunar repeat ground track orbits. Journal of Guidance, Control, and Dynamics **30**(4), 982–993 (2007)

[11] Beckman, M., Lamb, R.: Stationkeeping for the Lunar Reconnaissance Orbiter (LRO). In: Proceedings of the 20th International Symposium on Space Flight Dynamics, Annapolis, MD (2007)

[12] Knežević, Z., Milani, A.: An analytical perturbation theory for the low lunar polar orbiter. Publications de l'Observatoire Astronomique de Beograd **49**, 19–39 (1995)

[13] Knežević, Z., Milani, A.: Orbit maintenance of a lunar polar orbiter. Planetary and Space Science **46**(11–12), 1605–1611 (1998)

[14] Lara, M., Ferrer, S., De Saedeleer, B.: Lunar analytical theory for polar orbits in a 50-degree zonal model plus third-body effect. The Journal of the Astronautical Sciences **57**(3), 561–577 (2009)

[15] Mastroianni, R., Legnaro, E., Efthymiopoulos, C.: Fully analytical propagator for lunar satellite orbits in closed form. Celestial Mechanics and Dynamical Astronomy **138**(4), 45 (2026)

[16] Mahajan, B.: Lunar satellite analytic theory with complete gravity and third-body perturbations. Part-I: Gravity harmonics and their coupling effects. The Journal of the Astronautical Sciences **73**(2), 30 (2026)

[17] De Saedeleer, B.: Analytical theory of a lunar artificial satellite with third body perturbations. Celestial Mechanics and Dynamical Astronomy **95**(1–4), 407–423 (2006)

[18] San-Juan, J.F., López, R., Pérez, I.: High-fidelity semianalytical theory for a low lunar orbit. Journal of Guidance, Control, and Dynamics **42**(1), 163–167 (2019)

[19] Efthymiopoulos, C., Tsiganis, K., Gkolias, I., Gaitanas, M., Yanez, C.: SELENA: Semi-analytical Integrator for Lunar Artificial Satellites. arXiv:2309.11904. Final report for CNES research activity R-S20/BS-0005-062 (2023)

[20] Legnaro, E., Efthymiopoulos, C.: Secular dynamics and the lifetimes of lunar artificial satellites under natural force-driven orbital evolution. Acta Astronautica **225**, 768–787 (2024)

[21] Lara, M.: Nonresonant tesseral coupling: shape matters. Celestial Mechanics and Dynamical Astronomy **137**(6), 41 (2025)

[22] Cook, G.E.: Perturbations of near-circular orbits by the Earth's gravitational potential. Planetary and Space Science **14**(5), 433–444 (1966)

[23] Cook, R.A.: The long-term behavior of near-circular orbits in a zonal gravity field. In: Astrodynamics 1991. Advances in the Astronautical Sciences, vol. 76, pp. 2205–2221. Univelt, San Diego, CA (1992). AAS Paper 91-463

[24] Deleflie, F., Métris, G., Exertier, P.: An analytical solution of the Lagrange equations valid also for very low eccentricities: Influence of a central potential. Celestial Mechanics and Dynamical Astronomy **94**(1), 105–134 (2006)

[25] Deleflie, F., Métris, G., Exertier, P.: Long-period variations of the eccentricity vector valid also for near circular orbits around a non-spherical body. Celestial Mechanics and Dynamical Astronomy **94**(1), 83–104 (2006)

[26] Kaula, W.M.: Theory of Satellite Geodesy: Applications of Satellites to Geodesy. Blaisdell Publishing Company, Waltham, MA (1966)

[27] Kaula, W.M.: Analysis of gravitational and geometric aspects of geodetic utilization of satellites. Geophysical Journal International **5**(2), 104–133 (1961)

[28] Tisserand, F.: Traité de Mécanique céleste vol. 1. Gauthier-Villars, Paris (1889)

[29] Cayley, A.: Tables of the developments of functions in the theory of elliptic motion. Memoirs of the Royal Astronomical Society **29**, 191–306 (1861)

[30] Giacaglia, G.E.O.: A note on Hansen's coefficients in satellite theory. Celestial Mechanics **14**(4), 515–523 (1976)

[31] Gooding, R.H., Wagner, C.A.: On the inclination functions and a rapid stable procedure for their evaluation together with derivatives. Celestial Mechanics and Dynamical Astronomy **101**(3), 247–272 (2008)

[32] Logan, J.D.: A First Course in Differential Equations, 3rd edn. Undergraduate

Texts in Mathematics. Springer, Cham (2015)

[33] CS GROUP and contributors: Orekit: An Accurate and Efficient Core Layer for Space Flight Dynamics Applications. Accessed 23 October 2026 (n.d.)

Statements and Declarations

Funding

R. Vazquez and A. S. Rivero gratefully acknowledge support by grant PID2023-147623OB-I00 funded by MICIU/AEI/10.13039/ 501100011033 and by "ERDF A way of making Europe". A. S. Rivero was funded by a FPU grant from the Spanish Ministry of Universities.

Competing interests

The authors declare that they have no known competing financial interests or personal relationships that could have appeared to influence the work reported in this paper.

Data Availability

The code used to generate the results of this paper is available at https://github.com/AnaSRivero/Lunar-satellites-mean-eccentricity-vector.git.

Authors contribution

A. S. Rivero: Conceptualization, Methodology, Software, Writing—original draft, Writing—review and editing; G. Baù: Conceptualization, Methodology, Software, Writing—original draft, Writing—review and editing; R. Vazquez: Conceptualization, Methodology, Software, Writing—original draft, Writing—review and editing.